PAPER

Non-axisymmetric equilibrium and stability using the ELITE stability code

To cite this article: M.S. Anastopoulos-Tzanis *et al* 2019 *Nucl. Fusion* **59** 126028

IOP Publishing | International Atomic Energy Agency Nuclear Fusion

Nucl. Fusion **59** (2019) 126028 (11pp) https://doi.org/10.1088/1741-4326/ab40ef

Non-axisymmetric equilibrium and stability using the ELITE stability code

M.S. Anastopoulos-Tzanis[1,2], B.D. Dudson[1], C.J. Ham[2], C.C. Hegna[3], P.B. Snyder[4] and H.R. Wilson[1,2]

[1] York Plasma Institute, Department of Physics, University of York, York, YO10 5DD, United Kingdom of Great Britain and Northern Ireland
[2] Culham Centre for Fusion Energy, Abingdon, Oxfordshire OX14 3DB, United Kingdom of Great Britain and Northern Ireland
[3] Departments of Engineering Physics and Physics, University of Wisconsin-Madison, Madison, WI 53706, United States of America
[4] General Atomics, San Diego, CA 92186-5608, United States of America

E-mail: michail.anastopoulostzanis@york.ac.uk

Received 5 February 2019, revised 28 August 2019
Accepted for publication 3 September 2019
Published 11 October 2019

Abstract

Linear perturbation theory is used to model the ideal magnetohydrodynamic stability of tokamak equilibria under the application of external 3D magnetic perturbations (Hegna 2014 *Phys. Plasmas* **21** 072502). We use the ELITE code (Wilson *et al* 2002 *Phys. Plasmas* **9** 1277) to produce both a linear plasma response, as well as the linear axisymmetric toroidal eigenmodes which are used as basis functions for the 3D perturbative stability analysis. The symmetry breaking produces coupling of modes with different toroidal mode number, n, leading to modification of the linear growth rates, and poloidal localisation of the non-axisymmetric peeling–ballooning mode at sufficiently large applied field.

Keywords: RMP ELM control, 3D MHD stability, plasma response

(Some figures may appear in colour only in the online journal)

1. Introduction

The efficient production of fusion power requires large pressure at the plasma core while retaining low pressure at the plasma edge, such that plasma facing components (PFCs) operate in an acceptable environment. Such pressure profiles are observed in high confinement mode (H-mode) plasmas. However, the establishment of a steep pressure gradient at the edge, the so called pedestal region, together with large bootstrap driven edge current density destabilises peeling–ballooning (PB) instabilities [1]. Those instabilities are manifested as edge localised modes (ELMs) which correspond to rapid bursts of particles and heat to PFCs, especially to the divertor of the reactor. For large tokamaks like ITER, unmitigated ELMs will be sufficiently large to deliver heat fluxes that exceed the melting point of tungsten [2], the main material of the divertor tiles. Therefore, ELM control methods are required to avoid damage of the reactor PFCs and exhaust region [3].

One method of ELM control that is widely applied to tokamaks around the world, and will be installed in ITER, uses non-axisymmetric magnetic perturbations (MPs) produced by magnetic coils placed around the plasma, typically inside the tokamak vessel. Experimental observations indicate two main operational states with these coils. One, ELM mitigation, where there is a decrease in energy loss per ELM ΔW_{ELM} and an increase of ELM frequency f_{ELM}. The other, ELM suppression, i.e. no ELMs. For ITER-like shape low density $n/n_{\mathrm{GW}} \sim 0.3$, where $n_{\mathrm{GW}} = I_{\mathrm{p}}/\pi a^2$ is the Greenwald density limit, I_{p} the plasma current and a the minor radius, and low collisionality $\nu^* \sim 0.01$, complete suppression has been observed at DIII-D [4] and ASDEX Upgrade [5], while for higher collisionality $\nu^* \sim 1$ KSTAR [6] has also achieved ELM suppression—collisionality is the ratio between collision frequency and the characteristic bounce frequency of trapped particles. The exact physics mechanism that allows this ELM free regime is still to be understood. ITER will operate in a high Greenwald fraction $n/n_{\mathrm{GW}} \sim 0.7$, low

collisionality $\nu^* \sim 0.01$ regime which makes extrapolation from current machines challenging in the absence of a rigorous physics basis.

External 3D fields affect transport and magnetohydrodynamic (MHD) properties of the plasma. The resonant component of the field drives current structures at flux surfaces where the safety factor q is rational. Under certain conditions these can lead to magnetic islands, which greatly increase cross-field transport [7–9]. As a result, the pressure gradient in the pedestal is relaxed below global stability boundaries. However, plasma flow in the pedestal region can be strong enough for island structures to heal [10–13]. In addition, equilibrium geometry can influence MHD stability boundaries, and so affect the onset of ELMs. An infinite toroidal mode numbner n or local ballooning analysis reveals that the dominant effect of the applied 3D field is to alter the local magnetic shear, which has significant consequences for ideal MHD stability [14–16]. However, for the intermediate n modes, responsible for the occurrence of ELMs, a global 3D analysis is needed. Global 3D stability codes exist [17–20] but simulations of ideal MHD stability of medium to high n modes under the application of MPs are extremely challenging. Simulations performed with non-linear fluid codes demonstrate that toroidal mode coupling is one of the key mechanisms to influence the growth rate of unstable PB modes [21, 22].

The work presented here focuses on the impact of toroidal symmetry breaking on the ideal MHD stability of the plasma. In a toroidally axisymmetric system, the linear response is described by decoupled toroidal modes, i.e. toroidal mode number n, is a 'good quantum number' and only poloidal mode number coupling occurs. We consider an additional non-axisymmetric part of the equilibrium $B_N^{(1)}$, where N is the (assumed single) toroidal mode number of the imposed 3D field, that is much smaller than the axisymmetric part $B_0^{(0)}$; typically $B_N^{(1)}/B_0^{(0)} \sim 10^{-4}$, so linear perturbation theory can be employed to provide the required geometrical coupling of the axisymmetric modes. This coupling will result in energy transfer between neighbouring toroidal Fourier modes that can directly affect the evolution of instabilities. In this paper, we will explore this coupling mechanism.

2. Perturbative MHD stability framework

2.1. Features of perturbative MHD

A perturbative stability analysis has been performed to first order in [23] to approximate changes in axisymmetric stability due to the presence of narrow island structures. However, second order corrections, as in [24], are required to capture perturbative non-axisymmetric effects. First, consider the momentum equation, which for simplicity in the formalism is normalised to the mass density ρ,

$$\mathbf{F}\vec{\xi}_n = \frac{\partial^2}{\partial t^2}\vec{\xi}_n \Rightarrow (\mathbf{F}^{(0)} + \epsilon\mathbf{F}^{(1)} + \epsilon^2\mathbf{F}^{(2)} + ...)\vec{\xi}_n = -\omega_n^2\vec{\xi}_n \tag{1}$$

produced from a plasma displacement $\vec{\xi}_n$, where $\mathbf{F}^{(0)}$ is a force operator due to the axisymmetric equilibrium, $\mathbf{F}^{(k)}$ is a force operator due to axisymmetric and non-axisymmetric equilibrium changes of order k and ϵ represents a small parameter proportional to $B_N^{(1)}/B_0^{(0)} \ll 1$. Equation (1) represents an eigenvalue equation, where the set of $-\omega_n^2$ and $\vec{\xi}_n$ represent the eigenvalues (frequency or growth rate) and eigenfunctions (perpendicular displacement) respectively. Due to the perturbative nature of the higher order contributions the eigenvalues and eigenvectors can be expanded in the small parameter ϵ:

$$\omega_n^2 = \omega_n^{(0)2} + \epsilon\omega_n^{(1)2} + \epsilon^2\omega_n^{(2)2} + ... \tag{2}$$

$$\vec{\xi}_n = \vec{\xi}_n^{(0)} + \epsilon\vec{\xi}_n^{(1)} + \epsilon^2\vec{\xi}_n^{(2)} + ... \tag{3}$$

Solving order by order, we derive to $k \leqslant 2$,

$$\underline{0^{\text{th}}\text{ Order :}}\ \mathbf{F}^{(0)}\vec{\xi}_n^{(0)} = -\omega_n^{(0)2}\vec{\xi}_n^{(0)} \tag{4}$$

$$\underline{1^{\text{st}}\text{ Order :}}\ \mathbf{F}^{(1)}\vec{\xi}_n^{(0)} + \mathbf{F}^{(0)}\vec{\xi}_n^{(1)} = -\omega_n^{(1)2}\vec{\xi}_n^{(0)} - \omega_n^{(0)2}\vec{\xi}_n^{(1)} \tag{5}$$

$$\underline{2^{\text{nd}}\text{ Order :}}\ \mathbf{F}^{(2)}\vec{\xi}_n^{(0)} + \mathbf{F}^{(1)}\vec{\xi}_n^{(1)} + \mathbf{F}^{(0)}\vec{\xi}_n^{(2)} = -\omega_n^{(2)2}\vec{\xi}_n^{(0)} - \omega_n^{(1)2}\vec{\xi}_n^{(1)} - \omega_n^{(0)2}\vec{\xi}_n^{(2)}. \tag{6}$$

The unperturbed system

$$\mathbf{F}^{(0)}\vec{\xi}_n^{(0)} = -\omega_n^{(0)2}\vec{\xi}_n^{(0)} \tag{7}$$

is considered to be unstable and non-degenerate, i.e. $\omega_n^{(0)} \neq \omega_m^{(0)}$ for $n \neq m$. Thus, the eigenvalues $-\omega_n^{(0)2}$ and eigenfunctions $\vec{\xi}_n^{(0)}$ are fully determined for a range of n and can be used as basis functions for the solution of higher order equations. These basis functions are orthogonal, and considered to be normalised such that $\langle\vec{\xi}_m^{(0)}|\vec{\xi}_n^{(0)}\rangle = \int \vec{\xi}_m^{\dagger(0)} \cdot \vec{\xi}_n^{(0)}\mathcal{J}\mathrm{d}^3\mathbf{x} = \delta_{nm}$, where $\mathcal{J}$ is a weight function representing the Jacobian of the coordinate system.

To obtain first order corrections for the eigenvalues and eigenfunctions, the inner product of equation (5) with $\vec{\xi}_n^{(0)}$ is considered,

$$\langle\vec{\xi}_n^{(0)}|\mathbf{F}^{(0)}|\vec{\xi}_n^{(1)}\rangle + \langle\vec{\xi}_n^{(0)}|\mathbf{F}^{(1)}|\vec{\xi}_n^{(0)}\rangle = -\omega_n^{(0)2}\langle\vec{\xi}_n^{(0)}|\vec{\xi}_n^{(1)}\rangle - \omega_n^{(1)2}\langle\vec{\xi}_n^{(0)}|\vec{\xi}_n^{(0)}\rangle. \tag{8}$$

The first terms on the left and right hand sides of equation (8) cancel, due to the fact that $\mathbf{F}^{(0)}$ is Hermitian. This leads to a simple relation for the first order correction of the eigenvalue,

$$\omega_n^{(1)2} = -\langle\vec{\xi}_n^{(0)}|\mathbf{F}^{(1)}|\vec{\xi}_n^{(0)}\rangle. \tag{9}$$

Taking the inner product of equation (5) with $\vec{\xi}_m^{(0)}$ $(m \neq n)$ leads to

$$(\omega_m^{(0)2} - \omega_n^{(0)2})\langle\vec{\xi}_m^{(0)}|\vec{\xi}_n^{(1)}\rangle = \langle\vec{\xi}_m^{(0)}|\mathbf{F}^{(1)}|\vec{\xi}_n^{(0)}\rangle. \tag{10}$$

One can use the freedom in the solution to equation (5) for $\vec{\xi}_n^{(1)}$ to satisfy an orthogonality relation $\langle\vec{\xi}_n^{(0)}|\vec{\xi}_n^{(1)}\rangle = 0$. This allows the representation of the perturbed state as a superposition of the unperturbed states,

$$\vec{\xi}_n^{(1)} = \sum_{m\neq n} \langle \vec{\xi}_m^{(0)} | \vec{\xi}_n^{(1)} \rangle \vec{\xi}_m^{(0)}. \tag{11}$$

Substituting equation (11) into equation (10) provides the first order correction of the eigenfunction that depends on known quantities,

$$\vec{\xi}_n^{(1)} = \sum_{m\neq n} \frac{\langle \vec{\xi}_m^{(0)} | \mathbf{F}^{(1)} | \vec{\xi}_n^{(0)} \rangle}{(\omega_m^{(0)2} - \omega_n^{(0)2})} \vec{\xi}_m^{(0)}. \tag{12}$$

At this stage it can be noted that if the first order correction of the force operator $\mathbf{F}^{(1)}$ is non-axisymmetric, then the correction to the eigenfunction is non-zero $\vec{\xi}_n^{(1)} \neq 0$, but there is no change to the eigenvalue, i.e. $\omega_n^{(1)2} = 0$. On the other hand, if the first order correction of the force operator $\mathbf{F}^{(1)}$ is axisymmetric, the opposite is expected. In addition, for a non-axisymmetric magnetic perturbation with a toroidal mode number N, a triplet mode emerges: $\{n-N, n, n+N\}$. This leads to a poloidal localisation of the 3D mode, provided the coupling is strong enough.

In order to calculate corrections to either the mode structure or the growth rate of peeling–ballooning modes due to the presence of 3D fields, second order corrections need to be considered. Repeating the above procedure for equation (6), we derive:

$$\omega_n^{(2)2} = -\langle \vec{\xi}_n^{(0)} | \mathbf{F}^{(2)} | \vec{\xi}_n^{(0)} \rangle - \langle \vec{\xi}_n^{(0)} | \mathbf{F}^{(1)} | \vec{\xi}_n^{(1)} \rangle. \tag{13}$$

The second order force operator $\mathbf{F}^{(2)}$ can be dropped from the analysis as it provides corrections due to axisymmetric changes, and substituting equation (12) into equation (13), the second order correction of the eigenvalue is explicitly expressed as

$$\begin{aligned}\omega_n^{(2)2} &= -\sum_{m\neq n} \frac{\langle \vec{\xi}_n^{(0)} | \mathbf{F}^{(1)} | \vec{\xi}_m^{(0)} \rangle \langle \vec{\xi}_m^{(0)} | \mathbf{F}^{(1)} | \vec{\xi}_n^{(0)} \rangle}{(\omega_m^{(0)2} - \omega_n^{(0)2})} \\ &= -\sum_{m\neq n} \frac{||\mathbf{F}_{nm}^{(1)}||^2}{(\omega_m^{(0)2} - \omega_n^{(0)2})}.\end{aligned} \tag{14}$$

For a single toroidal mode number N, equation (12) and (14) result in solely in first neighbour coupling $m = n \pm N$, leading to the triplet mode $\{n-N, n, n+N\}$. Note that since the numerator of equation (14) is always positive, for $\omega_m^{(0)2} > \omega_n^{(0)2}$ the contribution is stabilising, while for $\omega_m^{(0)2} < \omega_n^{(0)2}$ the contribution is destabilising. Most importantly, if the spectrum contains extrema, the most unstable mode will become more unstable and the most stable mode becomes more stable.

The above method provides corrections to the mode structure and growth rate of unstable peeling–ballooning modes provided the total 3D equilibrium configuration and axisymmetric peeling–ballooning eigenfunctions are known. The total 3D equilibrium can be obtained from any linear or nonlinear 3D equilibrium code, for example VMEC [25], or considering the linear plasma response as can be provided by axisymmetric stability codes like MARS [26], IPEC [27], etc. In this work, the low n version of the stability code ELITE [28, 29] is used. ELITE is an axisymmetric eigenvalue ideal MHD stability code that can efficiently calculate the PB instability from low to high n toroidal modes. In addition, because the code solves for a displacement functional that minimises the perturbed potential energy, it can also provide the linear plasma response in marginal stability, i.e. assuming negligible inertial, provided an appropriate boundary condition is imposed at the plasma-vacuum interface. ELMs are a medium to high n ideal MHD phenomenon and no global ideal 3D MHD stability code has been used to resolve the effect of MPs on the stability of these modes, since the resolution required in the poloidal and toroidal direction is significant. The perturbative approach allows the examination of individual triplets that simplify the numerical complexity of the problem. The aim of this work is to be able to routinely produce stability diagrams for shots with applied MPs as is done currently with ELITE for axisymmetric shots. This is the first stage of a project to develop a tool which can optimise plasma response and ELM stability together.

2.2. Linear perturbed equilibrium

We adopt an axisymmetric orthogonal flux coordinate system $(\psi_0, \theta_0, \phi_0)$, where the poloidal flux ψ_0 serves as the normal to the axisymmetric flux surface coordinate and (θ_0, ϕ_0) define the axisymmetric orthogonal poloidal and toroidal angles. For this analysis only the perpendicular component $\vec{\xi}_\perp$ of the displacement is retained. The parallel displacement $\vec{\xi}_{||}$ produces no force for an incompressible plasma and in general is found to be significantly smaller than the perpendicular displacement such that it does not contribute in the inertia of the system. For those reasons, the parallel displacement is not required and the displacement under consideration takes the form,

$$\vec{\xi}_n^{(0)} = X_n^{(0)} \frac{\nabla\psi_0^{(0)}}{|\nabla\psi_0^{(0)}|^2} + U_n^{(0)} \frac{\nabla\psi_0^{(0)} \times \vec{B}_0^{(0)}}{B_0^{(0)2}}. \tag{15}$$

The binormal component of the displacement, U, can be expressed in terms of the normal component X:

$$\begin{aligned}[\frac{B_{\phi 0}^{(0)}}{B_0^{(0)2}} (\vec{B}_0^{(0)} \cdot \nabla) - in] U_n^{(0)} =& [\partial_{\psi_0} + \partial_{\psi_0} \ln(\mathcal{J}_0^{(0)} B_0^{(0)2}) \\ &+ 2\mu_0 \frac{\partial_{\psi_0} P_0^{(0)}}{B_0^{(0)}}] X_n^{(0)}.\end{aligned} \tag{16}$$

For a given toroidal mode number n, ELITE solves an eigenvalue equation for the set of poloidal Fourier harmonics, $X_{nl}(\theta_0^*)$, of the normal displacement. From these one can reconstruct the component of the displacement normal to flux surfaces:

$$X_n^{(0)} = \sum_l X_{nl}^{(0)} \exp[-\mathrm{i}(l\theta_0^* - n\phi_0)]. \tag{17}$$

The straight field line angle θ_0^* can be computed form the local magnetic pitch $\nu_0^{(0)}$, such that

$$\theta_0^* = \frac{1}{q^{(0)}}\int_0^{\theta_0} \nu_0^{(0)}\,\mathrm{d}\theta_0 = \frac{1}{q^{(0)}}\int_0^{\theta_0} \frac{\vec{B}_0^{(0)}\cdot\nabla\phi_0^{(0)}}{\vec{B}_0^{(0)}\cdot\nabla\theta_0^{(0)}}\,\mathrm{d}\theta_0. \quad (18)$$

The perturbation is inserted into ELITE as a fixed boundary condition at the plasma–vacuum interface. As long as the plasma surface is not a rational surface of the applied field, magnetic induction is used to link the covariant normal field $B_{\psi_0 N}^{(1)}$ at the plasma boundary to the normal displacement $X_N^{(1)}$ as given by

$$X_{Nl}^{(1)} = -\frac{iq^{(0)}\mathcal{J}^{(0)}}{\nu^{(0)}g_{\psi\psi}^{(0)}}\frac{B_{\psi_0\, Nl}^{(1)}}{(l-Nq^{(0)})} \quad (19)$$

where $\mathcal{J}^{(0)}$ is the Jacobian, $g_{\psi\psi}^{(0)} = 1/|\nabla\psi_0^{(0)}|^2$ is the covariant metric of the normal coordinate and (l,N) are the poloidal and toroidal mode numbers of the MP field. This method is an approximate as the correct boundary condition should be specified in terms of currents in the MP coils rather than a perturbed flux at the plasma boundary. Nevertheless, this approximation is sufficient to investigate the impact of the 3D fields on the plasma stability as discussed here. In order to calculate the 3D equilibrium fields, the total perpendicular displacement $\vec{\xi}_{\perp N}^{\,(1)}$ is required. Since ELITE provides the radial profiles of the poloidal harmonics of the normal displacement, the binormal displacement can be obtained considering equation (16).

Once the total perpendicular displacement $\vec{\xi}_{\perp N}^{\,(1)}$ is computed, the magnetic induction $\vec{B}_N^{(1)} = \nabla\times(\vec{\xi}_{\perp N}^{\,(1)}\times\vec{B}_0^{(0)})$ can be used to obtain the 3D components of the equilibrium magnetic field. Using a similar representation for the coordinate system in terms of the axisymmetric $(\nabla\psi_0^{(0)}, \nabla\psi_0^{(0)}\times\vec{B}_0^{(0)}, \vec{B}_0^{(0)})$, the 3D components of the magnetic field become

$$\vec{B}_N^{(1)} = B_{\psi_0 N}^{(1)}\frac{\nabla\psi_0^{(0)}}{|\nabla\psi_0^{(0)}|^2} + B_{s_0 N}^{(1)}\frac{\nabla\psi_0^{(0)}\times\vec{B}_0^{(0)}}{B_0^{(0)2}} + B_{b_0 N}^{(1)}\frac{\vec{B}_0^{(0)}}{B_0^{(0)2}} \quad (20)$$

$$B_{\psi_0 N}^{(1)} = (\vec{B}_0^{(0)}\cdot\nabla)X_N^{(1)} \quad (21)$$

$$B_{s_0 N}^{(1)} = (\vec{B}_0^{(0)}\cdot\nabla)U_N^{(1)} - S^{(0)}X_N^{(1)} \quad (22)$$

$$B_{b_0 N}^{(1)} = -B_0^{(0)2}(\nabla\cdot\vec{\xi}_{\perp N}^{\,(1)} + 2\vec{\xi}_{\perp N}^{\,(1)}\cdot\vec{\kappa}_0^{(0)}) + \vec{\xi}_{\perp N}^{\,(1)}\cdot\nabla P_0^{(0)} \quad (23)$$

where $S^{(0)} = -(\nabla\psi_0^{(0)}\times\vec{B}_0^{(0)}/|\nabla\psi_0^{(0)}|^2)\cdot\nabla\times(\nabla\psi_0^{(0)}\times\vec{B}_0^{(0)}/|\nabla\psi_0^{(0)}|^2)$ is the local magnetic shear and $\vec{\kappa}_0^{(0)} = \hat{b}_0^{(0)}\cdot\nabla\hat{b}_0^{(0)}$ is the magnetic curvature, with $\hat{b}_0^{(0)} = \vec{B}_0^{(0)}/B_0^{(0)}$.

2.3. Perturbative coupling coefficients

The calculation of the correction terms requires a knowledge of the perturbed force as resulting from the 3D equilibrium. Considering an ideal and incompressible plasma, a displacement $\vec{\xi}_n$ of the plasma will result in a force,

$$\vec{F} = \vec{J}\times\delta\vec{B}_n + \delta\vec{J}_n\times\vec{B} + \nabla(\vec{\xi}_n\cdot\nabla P) \quad (24)$$

where the quantities without index represent equilibrium quantities and $(\vec{\xi}_n,\ \delta\vec{B}_n,\ \delta\vec{J}_n)$ represent the mode displacement, magnetic field and current density respectively. In order to express $\vec{F}$ in an ordered way, the equilibrium can be split into an axisymmetric and non-axisymmetric part, i.e. $\vec{B} = \vec{B}_0^{(0)} + \vec{B}_N^{(1)}$. As such, ordering of the force operator results in

$$\vec{F}^{(0)} = \vec{J}_0^{\,(0)}\times\delta\vec{B}_n^{(0)} + \delta\vec{J}_n^{(0)}\times\vec{B}_0^{(0)} + \nabla(\vec{\xi}_n^{\,(0)}\cdot\nabla P_0^{(0)}) \quad (25)$$

$$\vec{F}^{(1)} = \vec{J}_0^{\,(0)}\times\delta\vec{B}_{n\pm N}^{(1)} + \vec{J}_N^{\,(1)}\times\delta\vec{B}_n^{(0)} + \delta\vec{J}_n^{(0)}\times\vec{B}_N^{(1)} + \delta\vec{J}_{n\pm N}^{(1)}\times\vec{B}_0^{(0)} + \nabla(\vec{\xi}_n^{\,(0)}\cdot\nabla P_N^{(1)}) \quad (26)$$

$$\vec{F}^{(2)} = \vec{J}_N^{\,(1)}\times\delta\vec{B}_{n\pm N}^{(1)} + \delta\vec{J}_{n\pm N}^{(1)}\times\vec{B}_N^{(1)} \quad (27)$$

where $\delta\vec{B}_n^{(0)} = \nabla\times(\vec{\xi}_n^{\,(0)}\times\vec{B}_0^{(0)})$ and $\delta\vec{B}_{n\pm N}^{(1)} = \nabla\times(\vec{\xi}_n^{\,(0)}\times\vec{B}_N^{(1)})$. The zeroth order force is due to the original axisymmetric equilibrium and the first order arises due to the non-axisymmetric equilibrium that provides first neighbour coupling between the toroidal axisymmetric modes. The second order force leads to changes in the axisymmetric growth rate but is dropped from the calculation, as it is assumed that $\vec{F}^{(1)} \ll \vec{F}^{(2)}$.

The coupling coefficients $\mathbf{F}_{nm}^{(1)}$ can be calculated using the above 3D equilibrium quantities $(\vec{B}_N^{(1)}, \vec{J}_N^{\,(1)}, \nabla P_N^{(1)})$ and axisymmetric toroidal modes $\{\vec{\xi}_n^{\,(0)}\}$ obtained using ELITE. Considering equation (26) and taking the inner product with $\vec{\xi}_n^{\,(0)}$, after some algebraic manipulation the coupling coefficients $\mathbf{F}_{nm}^{(1)}$ are split into a volume and surface contribution, such as

$$\begin{aligned}\mathbf{F}_{nm\ \mathrm{volume}}^{(1)} = -\int &[\vec{\xi}_n^{\,(0)\dagger}\cdot(\vec{J}_N^{\,(1)}\times\delta\vec{B}_m^{(0)} + \delta\vec{J}_m^{(0)}\times\vec{B}_N^{(1)})] \\ &+ [\nabla\times(\vec{\xi}_n^{\,(0)\dagger}\times\vec{J}_0^{\,(0)})]\cdot(\vec{\xi}_m^{\,(0)}\times\vec{B}_N^{(1)}) \\ &- \delta\vec{J}_n^{\,(0)\dagger}\cdot(\vec{\xi}_m^{\,(0)}\times\vec{B}_N^{(1)})\,\mathrm{d}V \end{aligned} \quad (28)$$

$$\begin{aligned}\mathbf{F}_{nm\ \mathrm{surface}}^{(1)} = -\int &(\vec{\xi}_n^{\,(0)\dagger}\cdot\hat{n}_0^{(0)})[(\vec{\xi}_m^{\,(0)}\times\vec{B}_N^{(1)})\cdot\vec{J}_0^{\,(0)} \\ &- \delta\vec{B}_{m\pm N}^{(1)}\cdot\vec{B}_0^{(0)} + \vec{\xi}_m^{\,(0)}\cdot\nabla P_N^{(1)}] \\ &+ \delta\vec{B}_n^{\,(0)\dagger}\cdot[\vec{B}_N^{(1)}(\vec{\xi}_m^{\,(0)}\cdot\hat{n}_0^{(0)}) - \vec{\xi}_m^{\,(0)}(\vec{B}_N^{(1)}\cdot\hat{n}_0^{(0)})]\,\mathrm{d}S. \end{aligned} \quad (29)$$

In order to retain accurate numerics even for high toroidal and poloidal mode numbers a Fourier representation is retained as described in the above section.

Finally, screening currents that arise due to electron flow at rational surfaces block the corresponding resonant harmonics of the applied magnetic perturbation, and in the absence of resistivity lead to δ-function current layers. The calculation of those layers is subtle within a single fluid MHD model due to large Pfirsch–Schlüter currents but can be approximated from the jump of the normal derivative of the perturbed flux $\Delta_{Nl} = [(l-Nq^{(0)})/q^{(0)}][\![\partial_\psi X_{Nl}]\!]$ according to [30] and given by

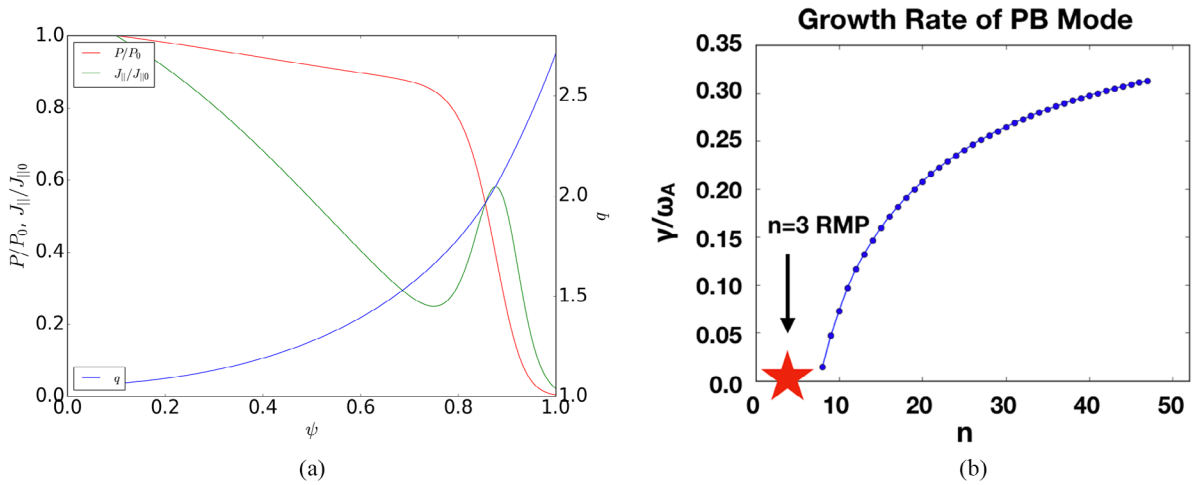

(a) (b)

Figure 1. Normalised radial equilibrium plasma profiles for (*a*) the pressure, outer mid-plane current density and q-profile as well as (*b*) the normalised PB growth rate for the *cbm*18_*dens*6 equilibrium.

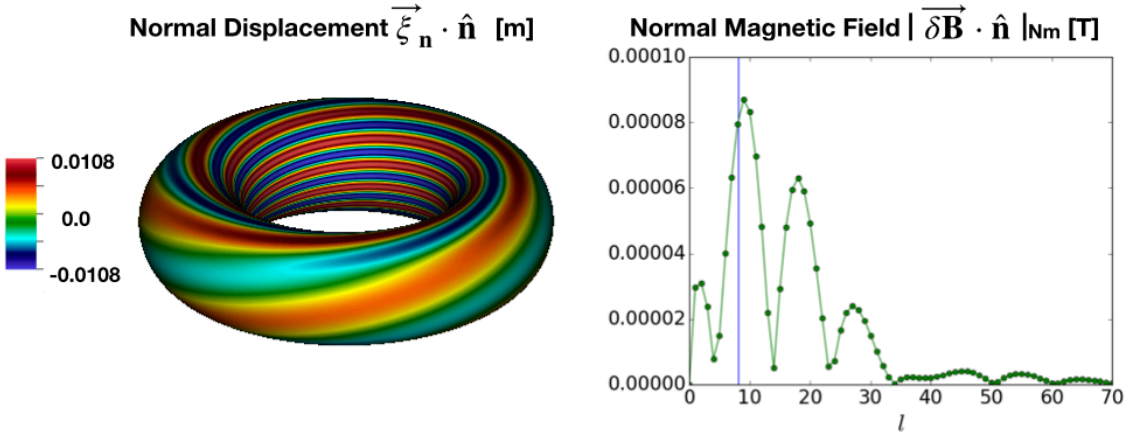

(a)

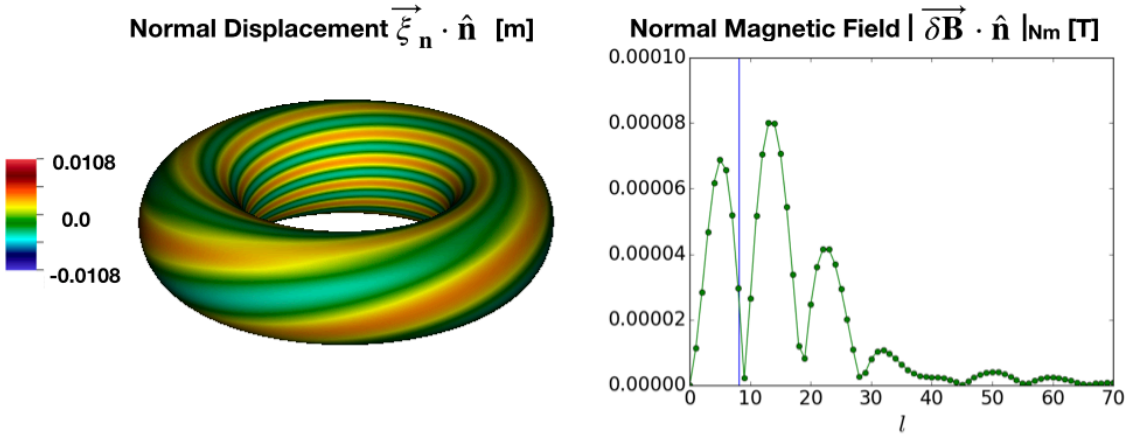

(b)

Figure 2. Normal displacement $\vec{\xi}_N^{(1)} \cdot \hat{n}_0^{(0)}$ (m) and Fourier decomposition of the normal magnetic field $\vec{B}_N^{(1)} \cdot \hat{n}_0^{(0)}$ (T) for the (*a*) resonant and (*b*) non-resonant $N = 3$ MP configuration at the plasma surface. The solid blue line represents the resonant location $q_a^{(0)} N = 8.13$ of the plasma surface.

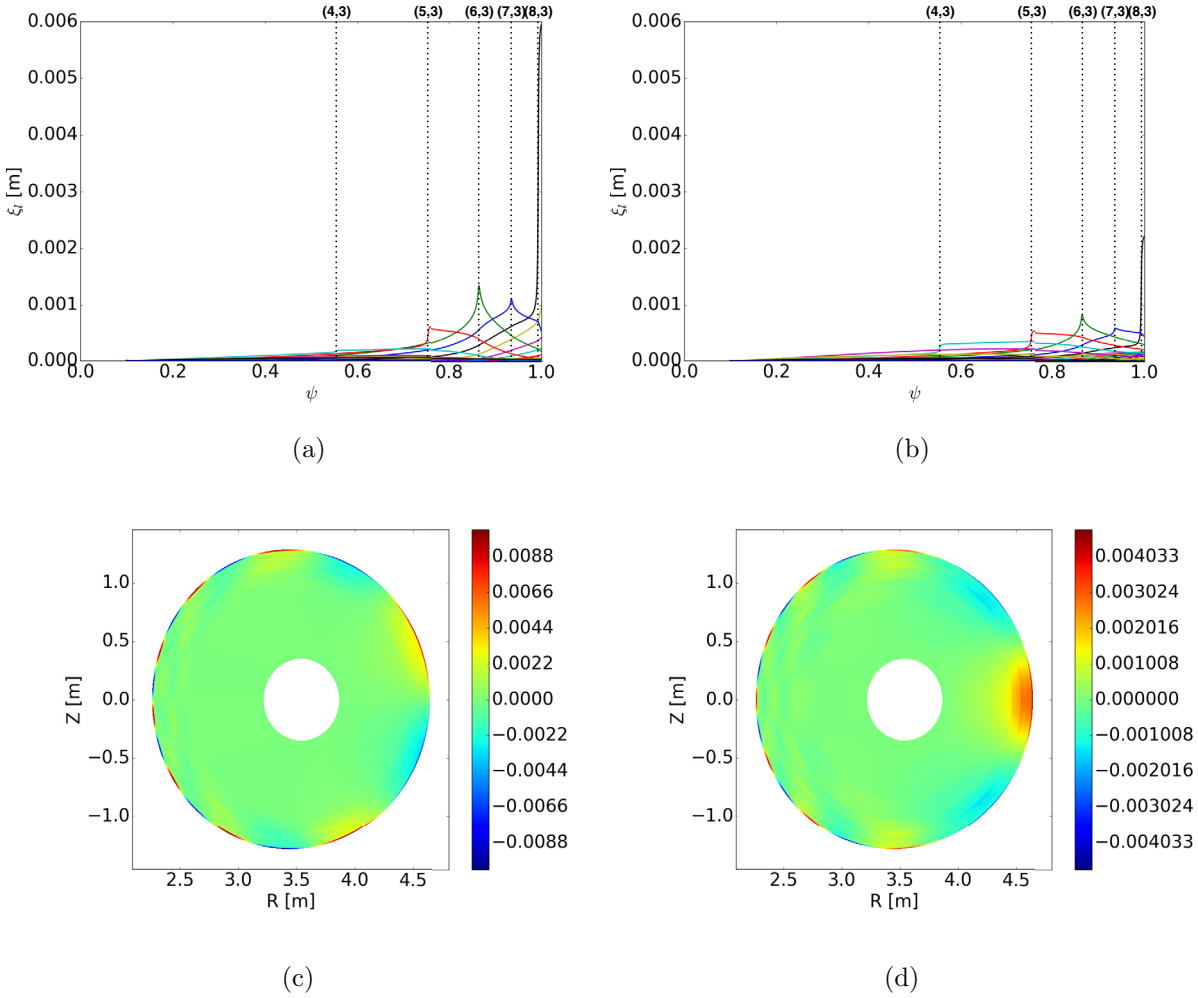

Figure 3. The radial dependence of the poloidal Fourier harmonics ξ_l for $l = [0, 70]$ of the normal displacement $\vec{\xi}_N^{(1)} \cdot \hat{n}_0^{(0)}$ (m) as a function of $\psi_0^{(0)}$ for (*a*) a resonant and (*b*) a non-resonant $N = 3$ MP field. The harmonics that peak around resonant surfaces are the corresponding resonant harmonics. In addition, the reconstruction of the poloidal cross section of the mode for the resonant (*c*) and non-resonant (*d*) case respectively.

$$\mu_0 \vec{J}^{(1)}_{||N\ \text{screening}} = -\sum_l \frac{l\Delta_{Nl}\delta(\psi^{(0)} - \psi_l^{(0)})}{n^2 \oint B_0^{(0)2}/|\nabla\psi_0^{(0)}|^2 \mathrm{dS}} \times \exp\left[-\mathrm{i}(l\theta_0^* - N\phi_0)\right]\vec{B}_0^{(0)} \quad (30)$$

where ψ_l corresponds to the poloidal flux at a rational surface. The corresponding coupling coefficients that arise from this contribution are given by

$$\mathbf{F}^{(1)}_{nm\ \text{screening}} = -\int \vec{\xi}_n^{(0)\dagger} \cdot (\vec{J}^{(1)}_{||N\ \text{screening}} \times \delta\vec{B}_m^{(0)})\, \mathrm{d}V. \quad (31)$$

3. Application to RMPs

The calculation of the non-axisymmetric part of the equilibrium begins with an initial axisymmetric equilibrium that is stable to low n toroidal modes but unstable to intermediate to high n ballooning modes, to which MP fields are applied. We examine such an equilibrium for a large aspect ratio circular cross-section plasma of core pressure $P_0^{(0)} = 22.8$ (kPa), core magnetic field $B_0^{(0)} = 1.8$ (T), core parallel current density $J_{||0}^{(0)} = 0.7$ (MAm^{-2}) and edge safety factor $q_a^{(0)} = 2.71$. The axisymmetric equilibrium plasma profiles and PB stability analysis are illustrated in figure 1.

3.1. Linear plasma responce to MPs

Two cases are examined, one for a resonant magnetic field and one for a non-resonant magnetic field at the plasma–vacuum interface for a toroidal mode number $N = 3$ MP field. Figure 2 illustrates the normal displacement $\vec{\xi}_N^{(1)} \cdot \hat{n}_0^{(0)}$ that represents the boundary condition, and the poloidal mode structure of the corresponding normal magnetic field $\vec{B}_N^{(1)} \cdot \hat{n}_0^{(0)}$, where $\hat{n}_0^{(0)} = \nabla\psi_0^{(0)}/|\nabla\psi_0^{(0)}|$ is the unit vector normal to the magnetic flux surfaces of the axisymmetric reference equilibrium.

In the resonant case the plasma response is characterised by a strong peeling-like normal displacement (strong edge

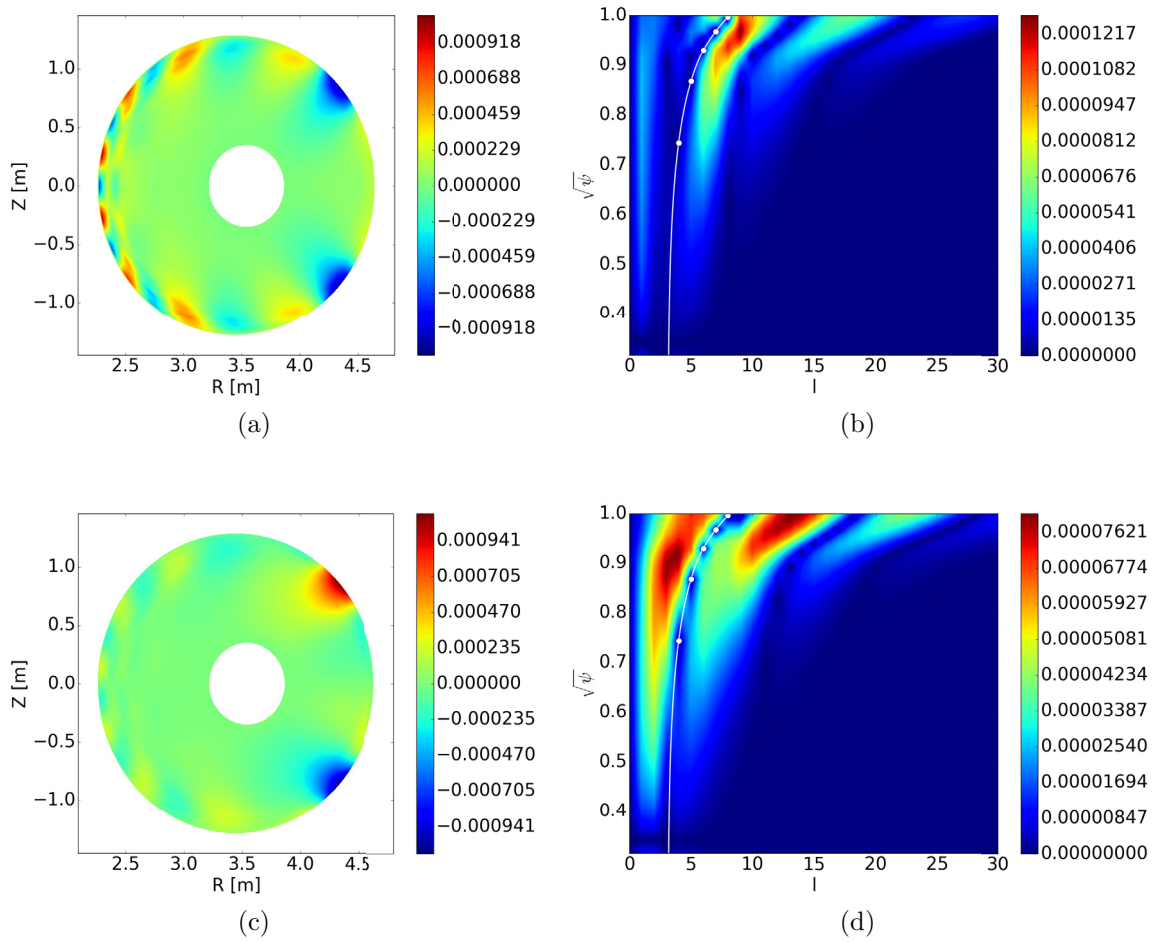

Figure 4. The (*a*), (*c*) normal component of magnetic field $\vec{B}_N^{(1)} \cdot \hat{n}_0^{(0)}$ (T) and (*b*), (*d*) its poloidal mode structure $B_{Nl}^{(1)}$ (T) in a straight field-line angle coordinate system as reconstructed from ELITE output data for (*a*), (*b*) a resonant and (*c*), (*d*) a non-resonant $N = 3$ MP configuration. The straight white line indicates the position of the q-profile.

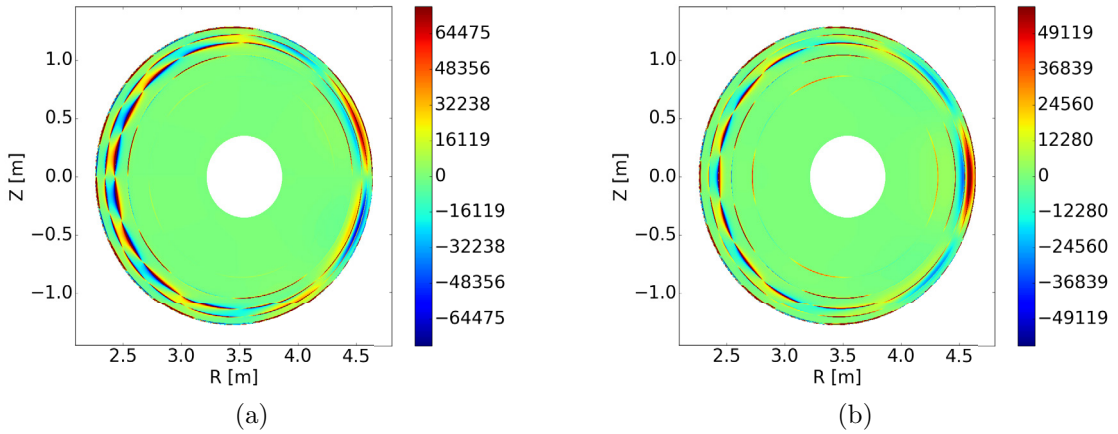

Figure 5. The parallel current density $J_{||N}^{(1)}$ (A m^{-2}) as reconstructed from ELITE output data for the (*a*) resonant and (*b*) non-resonant $N = 3$ MP configuration.

localisation), while in the non-resonant case a kink-ballooning response is observed (penetration further inside the plasma). The normal displacement is strongly peaked around rational surfaces in both cases, due to resonance with the corresponding poloidal harmonics, leading to large local response and potential break down of the linear response. Although, away from the rational surfaces $(\vec{\xi}_N^{(1)} \cdot \hat{n}_0^{(0)})/R_0^{(0)} \sim (\vec{B}_N^{(1)} \cdot \hat{n}_0^{(0)})/B_0^{(0)}$, such that a linear response is valid in the majority of the plasma volume and in many cases is observed to match with a non-linear plasma response model [31]. The mode structure and

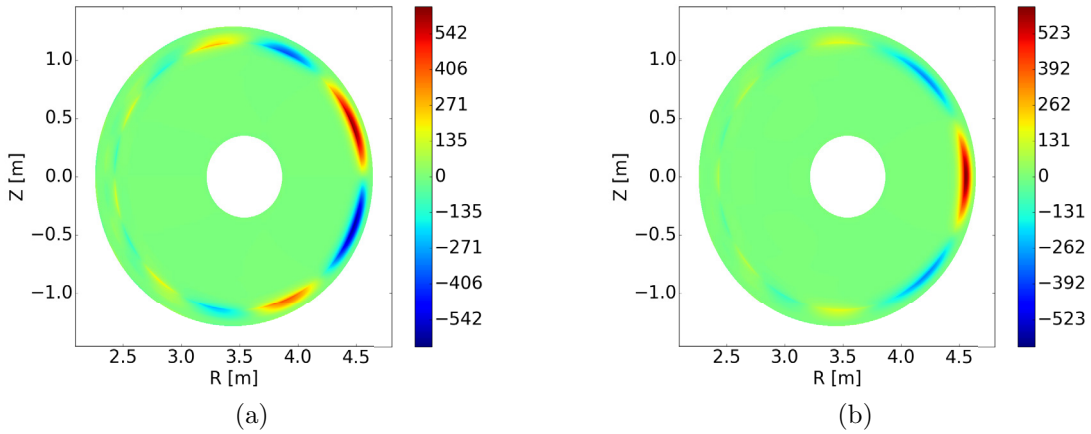

Figure 6. The plasma pressure $P_N^{(1)}$ (Pa) as reconstructed from ELITE output data for the (*a*) resonant and (*b*) non-resonant $N = 3$ MP configuration.

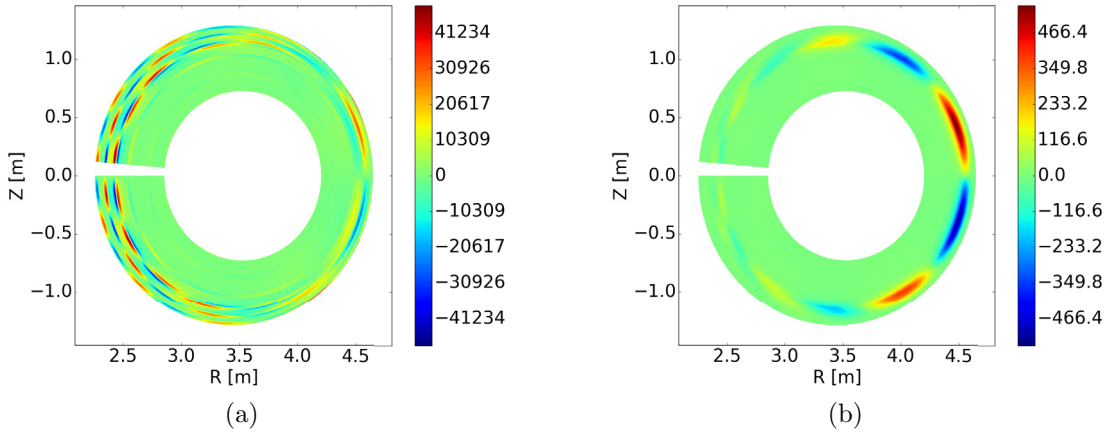

Figure 7. The (*a*) parallel current density $J_{||N}^{(1)}$ (A m^{-2}) and (*b*) plasma pressure $P_N^{(1)}$ (Pa) as calculated from BOUT++ for the resonant $N = 3$ MP configuration.

the poloidal cross-section reconstruction of the normal displacement are depicted in figure 3.

In this ideal MHD model, individual poloidal harmonics of the normal magnetic field are screened at their corresponding rational surfaces so that island formation is prohibited, since field line bending is minimised, i.e. $(\vec{B}_0^{(0)} \cdot \nabla) \propto (l - Nq^{(0)}) = 0$. Nevertheless, this screening is imperfect due to poloidal coupling in toroidal geometry. In the non-resonant case, this screening effect is reduced since the poloidal harmonics of the vacuum MP field are already minimised at the rational surfaces. However, in the resonant case the harmonics of the vacuum MP field are maximised at the rational surfaces and strong screening is observed, leading to significant modification of the prior MP vacuum field. The normal field and its poloidal mode structure are illustrated in figure 4.

The calculation of the current density becomes straight forward once the magnetic field and metrics of the coordinate system are known. Figure 5 illustrates the parallel current density $J_{||N}^{(1)}$ created around rational surfaces, which has two contributions. One contribution corresponds to the existence of Pfirsch–Schlüter current density due to quasi-neutrality and non-vanishing pressure gradient. The second contribution arises due to screening currents at rational surfaces. The ideal plasma response results in large Pfirsch–Schlüter current density for both MP configurations, which is the dominant contribution to the current density. The final perturbed quantity is the non-axisymmetric pressure calculated using the linearised perturbation $P_N^{(1)} = -\vec{\xi}_{\perp N}^{(1)} \cdot \nabla P_0^{(0)}$. For the toroidal mode coupling coefficients the pressure gradient $\nabla P_N^{(1)}$ is needed and obtained through the linearised force balance $\vec{J}_N^{(1)} \times \vec{B}_0^{(0)} + \vec{J}_0^{(0)} \times \vec{B}_N^{(1)} = \nabla P_N^{(1)}$. The non-axisymmetric pressure profile is shown in figure 6.

In order to verify that the computed non-axisymmetric equilibrium as resulted from ELITE is valid, BOUT++ [32] is used to model the linear plasma response imposing a fixed parallel magnetic potential $A_{||N}^{(1)}$ at the outer boundary of the computational domain. At first the $A_{||N}^{(1)}$ is computed using the original coordinate system $[\nabla\psi_0^{(0)}, \nabla\theta_0^{(0)}, \nabla\phi_0^{(0)}]$

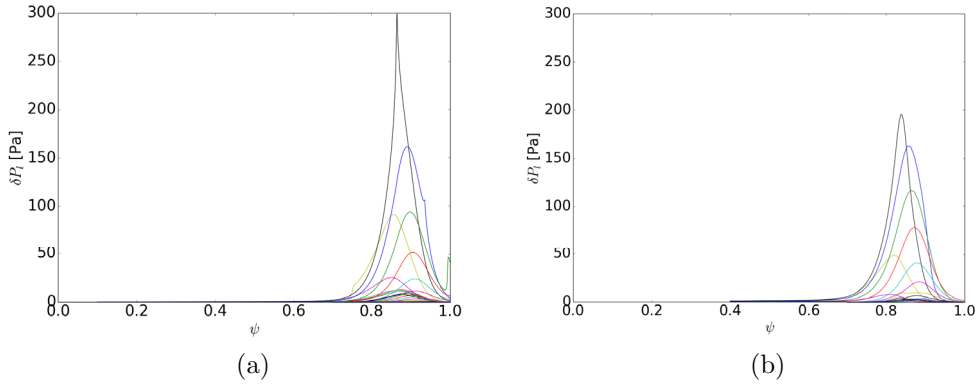

Figure 8. Comparison of the plasma pressure poloidal mode structure in the straight field line angle coordinate system between (*a*) ELITE and (*b*) BOUT++ results.

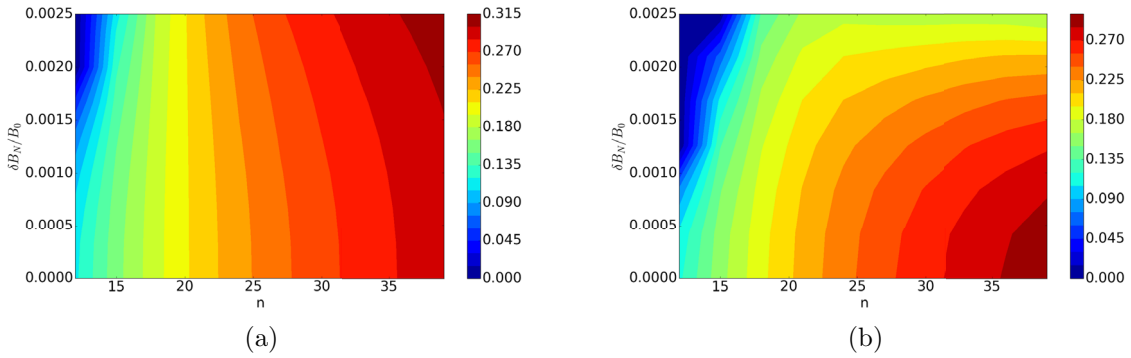

Figure 9. Perturbative 3D PB normalised growth rates γ/ω_A as a function of external $B_N^{(1)}/B_0^{(0)}$ and toroidal mode number n for (*a*) the resonant and (*b*) non-resonant $N = 3$ MP configuration.

and then transformed into a field aligned coordinate system $[\nabla\psi_0^{(0)}, \vec{B}_0^{(0)}, \nabla(\phi_0^{(0)} - q^{(0)}\theta_0^{(0)*})]$ that BOUT++ uses, employing the transformation $A_{||N}^{(1)} \equiv A_{||N}^{(1)} \exp[-\mathrm{i}(q^{(0)}N\theta_0^{(0)*})]$. The physics model under consideration is based on a reduced ideal MHD model appropriate for flute-like and incompressible perturbations, where more information can be found in [32] and [33]. As it can be observed from figures 7 and 8, the non-axisymmetric equilibrium pressure and parallel current density match well with ELITE. Some discrepancy occurs close to rational surfaces, which is attributed to the non-uniform grid spacing along the normal direction that allows very fine resolution close to rational surfaces with ELITE, and as a result sharper features can be resolved.

3.2. Impact of symmetry breaking on ideal MHD stability

Once the 3D equilibrium magnetic configuration and the axisymmetric peeling–ballooning eigenmodes are computed the corrections due to the MP can be obtained. Figure 9 shows the calculation of the normalised growth rate of the system for the resonant and non-resonant case. In the resonant case, it can be observed that the growth rate of unstable PB modes increases indicating further destabilisation and stronger coupling with the $m = n - N$ toroidal modes. However, it should be noted that the increase is small at experimentally relevant MP field amplitudes. On the other hand, in the non-resonant case it can be seen that the growth rate of unstable PB modes reduces, indicating stronger coupling with the $m = n + N$ toroidal modes and stabilisation of PB modes from the applied MP field. However, in both cases the lower n modes become more stable. In addition, the impact in the non-resonant case is stronger, even though the plasma response is smaller. Such a feature indicates the importance of the poloidal spectrum of the applied MP field, and not only its absolute magnitude, to influence plasma stability. Finally, 3D MHD stability indicates the existence of distinct mode families, i.e. coupling of a whole range of toroidal modes. However, the notion of mode families in this perturbative analysis is misleading, since weak coupling is assumed between the toroidal modes where only first neighbour coupling is retained. As a result the axisymmetric notion of distinct toroidal modes is preserved but replaced by the triplet mode $\{n - N, n, n + N\}$.

The reconstruction of the 3D normal displacement of the instability results in a concentration of the mode structure into distinct poloidal locations as can be observed from figure 10, due to the interplay of different primary poloidal harmonics from each toroidal eigenmode, provided that the coupling between these harmonics is strong enough. Specifically, the 3D mode is maximised between locations where the pressure gradient is amplified from the plasma response and the normal displacement of the plasma response crosses zero.

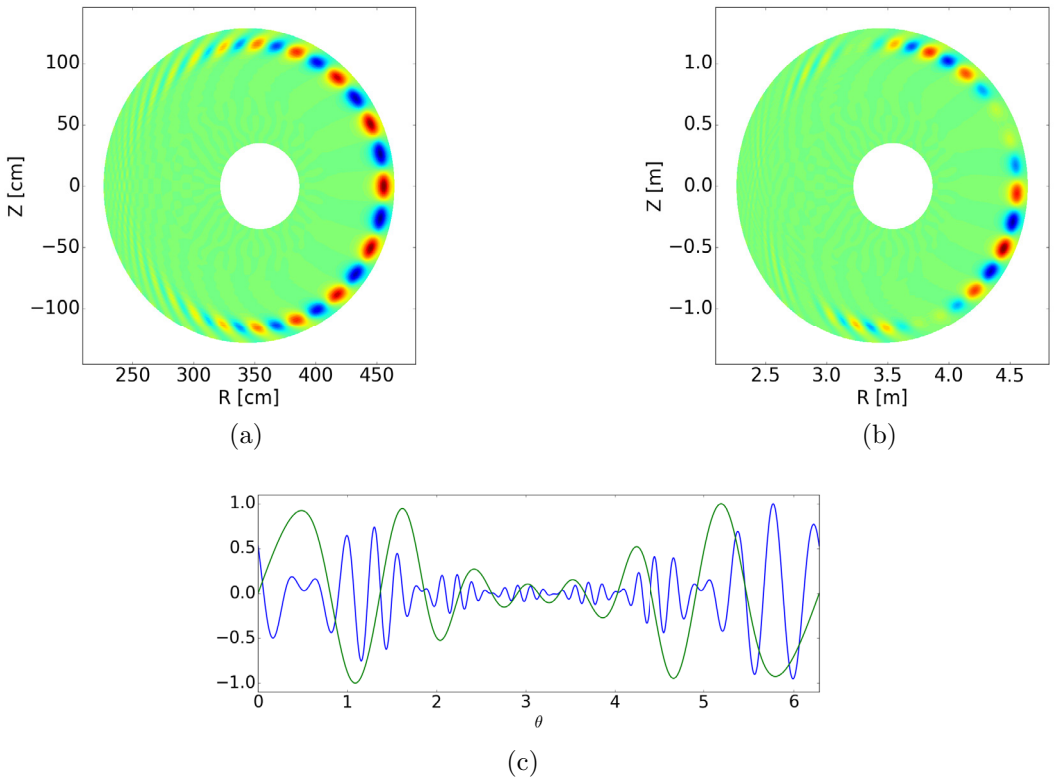

Figure 10. Comparison of the mode structure of a $n = 12$ unstable PB mode for (a) an axisymmetric equilibrium and (b) a non-axisymmetric equilibrium for the non-resonant $N = 3$ MP field of amplitude $B_N^{(1)}/B_0^{(0)} \sim 10^{-3}$. ($c$) Poloidal dependence of the normal displacement for the triplet mode (blue line) and the plasma response (green) at the radial location where the triplet mode is maximum.

4. Conclusion

To summarise, applied MP fields that break the axisymmetric nature of tokamak plasmas, are widely used to control ELMs. The 3D plasma stability can be studied in a perturbative way, as long as the full 3D equilibrium and the axisymmetric toroidal modes are known. The stability code ELITE has been used to obtain both the axisymmetric toroidal eigenmodes required for the toroidal coupling and also the fixed boundary linear plasma response to the applied MP field. In addition, screening current density is captured but has not been observed to have a strong impact on MHD stability. On the contrary, the 3D equilibrium profiles and the geometrically induced toroidal mode coupling had a significant impact on MHD modes above a certain phenomenological threshold for the amplitude of the applied field. We illustrate these results by perturbing an axisymmetric equilibrium, which is stable for $n < 8$, and has an increasing growth rate for $n \geqslant 8$. The growth rate is enhanced by the magnetic perturbation in the case of a resonant applied field, due to stronger coupling with the lower n sideband. On the other hand, decrease of the linear growth rate is observed due to stronger coupling with the higher n sideband of the axisymmetric system in the non-resonant case. It should be noted that in axisymmetric equilibria, where extrema exist in the growth rate spectrum, a variety of trends can exist. In addition, the absolute amplitude of the response is not the only key factor for efficient toroidal coupling, and consequent impact on the PB growth rates, i.e. the poloidal spectrum of the perturbation is also very important.

The coupling of toroidal harmonics can significantly influence the ballooning instability even for a low MP field of $B_N^{(1)}/B_0^{(0)} \sim 10^{-3}$. This then raises questions about the validity of our perturbative approach in which we couple toroidal eigenmodes, without taking into account the influence of the MP field on the axisymmetric mode structure of the triplet. In order to resolve such an issue, a more general variational approach can be followed using the individual poloidal and toroidal Fourier modes from the axisymmetric PB modes as a basis for trial functions, summing over both with coefficients to be determined by minimisation of the energy functional. This provides significantly more degrees of freedom, allowing the MP field to influence the ballooning structure of each constituent axisymmetric mode. Future work will focus on implementing such a variational formulation of the 3D stability and provide further insight regarding the physics mechanisms that allows an ELM-free operational state necessary for the advanced operation of ITER.

Acknowledgments

This work has been carried out within the framework of the EUROfusion Consortium and has received funding from the Euratom research and training programme 2014–2018 and 2019–2020 under Grant Agreement No. 633053 and from the RCUK Energy Programme (Grant No. EP/P012450/1) as well as the Fusion CDT Programme through the EPSRC (Grant No. EP/L01663X/1). To obtain further information

on the data and models underlying this paper please contact PublicationsManager@ukaea.uk. The views and opinions expressed herein do not necessarily reflect those of the European Commission. This research is also supported in part by the U.S. Department of Energy (DOE) Office of Fusion Energy Sciences under Grant No. DE-FG02-86ER53218.

ORCID iDs

M.S. Anastopoulos-Tzanis https://orcid.org/0000-0001-6564-3152
B.D. Dudson https://orcid.org/0000-0002-0094-4867
C.J. Ham https://orcid.org/0000-0001-9190-8310
P.B. Snyder https://orcid.org/0000-0002-0613-4232

References

[1] Connor J.W. *et al* 1998 *Phys. Plasmas* **5** 2687
[2] Pitts R.A. *et al* 2013 *J. Nucl. Mater.* **438** 48
[3] Loarte A. *et al* 2014 *Nucl. Fusion* **54** 033007
[4] Evans T.E. *et al* 2008 *Nucl. Fusion* **48** 024002
[5] Suttrop W.A. *et al* 2018 *Nucl. Fusion* **58** 096031
[6] Jeon Y.M. *et al* 2012 *Phys. Rev. Lett.* **109** 035004
[7] Fitzpatrick R. 1993 *Nucl. Fusion* **33** 7
[8] Hazeltine R.D. *et al* 1976 *Phys. Rev. Lett.* **37** 102
[9] Joseph I. *et al* 2008 *Nucl. Fusion* **48** 045009
[10] Liu Y.Q. *et al* 2011 *Nucl. Fusion* **51** 083002
[11] Becoulet M. *et al* 2012 *Nucl. Fusion* **52** 054003
[12] Waelbroeck F.L. *et al* 2012 *Nucl. Fusion* **52** 074004
[13] Fitzpatrick P. 2018 *Phys. Plasmas* **25** 112505
[14] Cote T.B. *et al* 2019 *Nucl. Fusion* **59** 016015
[15] Bird T.M. *et al* 2013 *Nucl. Fusion* **53** 013004
[16] Ham C.J. *et al* 2014 *Phys. Plasmas* **21** 102501
[17] Anderson D.V. *et al* 1990 *Int. J. High Perform. Comput. Appl.* **4** 3
[18] Nuehrenberg C. 1996 *Phys. Plasmas* **3** 2401
[19] Strumberger E. *et al* 2017 *Nucl. Fusion* **57** 016032
[20] Weyens T. *et al* 2017 *J. Comput. Phys.* **330** 997
[21] Orain F. *et al* 2015 *Plasma Phys. Control. Fusion* **57** 014020
[22] Orain F. *et al* 2019 *Phys. Plasmas* **26** 042503
[23] Helander P. *et al* 2013 *Phys. Plasmas* **20** 062504
[24] Hegna C.C. 2014 *Phys. Plasmas* **21** 072502
[25] Hirshman S.P. *et al* 1986 *Comput. Phys. Commun.* **43** 143
[26] Liu Y. *et al* 2010 *Phys. Plasmas* **17** 122502
[27] Park J.K. *et al* 2007 *Phys. Plasmas* **14** 052110
[28] Wilson H.R. *et al* 2002 *Phys. Plasmas* **9** 1277
[29] Lunniss A.E.L. 2016 Modelling eruptions and edge stability in tokamak plasmas *PhD Thesis* University of York (http://etheses.whiterose.ac.uk/id/eprint/16638)
[30] Park J.K. *et al* 2007 *Phys. Rev. Lett.* **99** 195003
[31] Willensdorfer M. *et al* 2016 *Plasma Phys. Control. Fusion* **58** 114004
[32] Dudson B.D. *et al* 2009 *Comput. Phys. Commun.* **180** 9
[33] Hazeltine R.D. *et al* 2003 *Plasma Confinement* (New York: Dover)